(Proceedings ModelCARE2011 held at Leipzig, Germany, in September 2011) (IAHS Publ. 355, 2012).

Modes of free convective flow in fractured-porous rock

KATHARINA VUJEVIĆ & THOMAS GRAF

Institute of Fluid Mechanics and Environmental Physics in Civil Engineering, Leibniz Universität Hannover, Appelstr. 9A, 30167 Hannover, Germany

vujevic@hydromech.uni-hannover.de

Abstract The effect of regular orthogonal fracture networks on density dependent free convection is investigated by numerical simulations. Discrete orthogonal fracture networks of different fracture spacing are systematically added to the Horton-Rogers-Lapwood (HRL) problem for free-convective flow in unfractured homogeneous porous rock. The equivalent hydraulic conductivity was preserved when fractures were added. Simulation results suggest that fractures affect free-convective flow if: (i) fracture permeability is more than five orders of magnitude larger than matrix permeability, and if (ii) fracture spacing is large. With decreasing fracture spacing, flow patterns approximate those of the corresponding unfractured HRL problem. Furthermore, a diffusion-only case at low Rayleigh number in homogeneous unfractured rock is regarded. It is shown that adding few fractures with large fracture spacing promotes free convective flow compared to the unfractured case of the same equivalent permeability.

Key words groundwater; fractures; Rayleigh; density; HydroGeoSphere; numerical modelling

MOTIVATION

In homogeneous aquifers with unstable groundwater density layering, cells of free convective flow may form whose number and shape depends, amongst other parameters, on the rock permeability and on the prevailing density gradient. The presence of open fractures may complicate the free convective flow mode as fractures represent preferential pathways where water flow velocities can be significantly larger than in the rock matrix itself. The aim of this study is therefore to determine the conditions under which fractures considerably influence free-convective flow. This is particularly important for questions concerning salt water intrusion into groundwater bodies near coasts or salt lakes, contaminant spreading near waste disposals or geothermal exploitation areas.

NUMERICAL MODELLING

Unfractured homogeneous HRL problem

The Horton-Rogers-Lapwood (HRL) problem is a well defined test scenario of free convective flow in unfractured homogeneous media illustrated in Fig. 1 (Horton & Rogers, 1945; Lapwood, 1948). The dimensionless Rayleigh number (Ra) can be used to determine the onset of convection. The Rayleigh number compares buoyancy that promotes free convection with diffusivity that dissipates free convection. If the density gradient is only due to salinity differences and if hydrodynamic dispersion is not considered, the Rayleigh number reads:

$$\mathrm{Ra} = \frac{\text{buoyancy}}{\text{diffusivity}} = \frac{\beta\,(\omega_{\max} - \omega_{\min})\,H\,k\,g\,\rho_0}{\theta\,\tau\,D_0\,\mu_0} \tag{1}$$

where β is the solute expansion coefficient, $\omega_{\max/\min}$ is the maximum/minimum salt mass fraction (kg kg^{-1}), H is the height of the domain (m), k is the permeability of the porous medium (m^2), g is the gravitational acceleration (m s^{-2}), ρ_0 is the reference fluid density (kg m^{-3}) and μ_0 is the reference fluid viscosity (kg m^{-1} s^{-1}). Diffusivity is composed of the free-solution diffusion coefficient D_0 (m^2 s^{-1}), the tortuosity τ (-), and the porosity θ (-).

The critical Rayleigh number Ra_c for the HRL problem is $4\pi^2$. This is to say, for $\mathrm{Ra} < 4\pi^2$, the system is purely diffusive and is called stable, whereas for $\mathrm{Ra} > 4\pi^2$, the system is dominated by buoyancy induced free convection and is called unstable. For high Rayleigh numbers the flow pattern of the HRL problem becomes increasingly sensitive to initial conditions and initial

perturbations. The present study is therefore limited to low Rayleigh numbers (60 and below). That restriction is in excellent agreement with studies on the Elder problem by van Reeuwijk *et al.* (2009). They found that "for Ra < 76, the Elder problem has a single steady state solution", and they therefore limited their studies to the Rayleigh number of 60.

Simulations are performed by using the numerical variable-density groundwater flow and transport model HydroGeoSphere (Therrien *et al*., 2010). The control volume finite element method is applied to the flow equation and a Galerkin finite element method is applied to the transport equation. Flow and transport are coupled because density variations cause nonlinearities in the flow equation. The coupled system of equations is linearized by a Picard scheme. Fractures are represented as discrete fractures that share common nodes with the adjacent matrix. Thus, for each node there is only one unknown for pressure (p) and salt mass fraction (ω), respectively. Fluid density is assumed to be a linear function of salinity. For further details on the HydroGeoSphere model, the reader is referred to Graf & Therrien (2007), and Therrien *et al.* (2010).

The conceptual model is shown in Fig. 1. Simulations are performed for a rectangular box with a height of 10 m, an aspect ratio (width to height) of 2, a thickness of one element and about 8000 elements in total. A grid refinement study was performed to ensure that this special discretization is adequate. The domain boundaries are impermeable, except two Dirichlet nodes at the upper left corner of the domain (front and back), where fluid pressure is zero. Lateral boundaries are assigned a zero-dispersive flux boundary condition, while bottom and top are Dirichlet boundaries with specified salt mass fractions of 0.0 and 0.1, respectively. Maximum fluid density is 1070 kg/m^3 at the top.

Initial conditions for the simulations are obtained by using simulation results of an unfractured HRL-problem with Rayleigh number 10 (no convection) as proposed by Weatherill *et al*. (2004), which corresponds to a linear decrease of both density and salinity. At the central node of the domain, an initial perturbation of the salinity field is applied by increasing the initial salt mass fraction by 10%. The homogeneous solute version of the unfractured HRL problem will be referred to as "base case". Its steady state solution for Rayleigh number 60 is presented in Fig. 2.

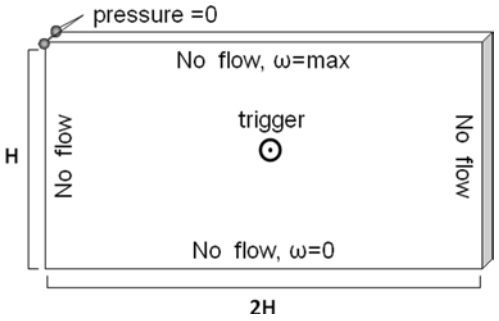

Fig. 1 Conceptual model of the unfractured HRL problem ("base case").

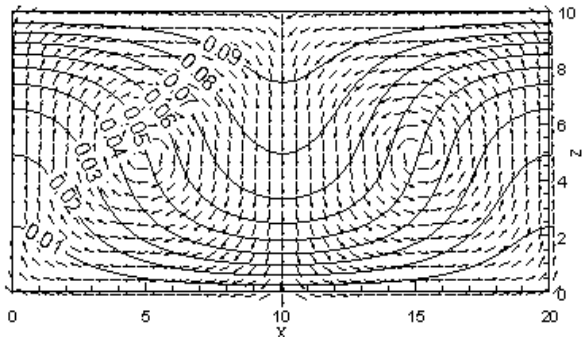

Fig. 2 Unfractured HRL problem – isochlors and standardized flow vectors for Rayleigh number 60.

Fractured HRL problem

An equidistant, orthogonal network of discrete fractures is added to the base case. Lateral boundaries are chosen such that they coincide with the location of fractures. The reason is that fracture flow is predominantly along the fracture due to its high conductivity and, therefore, fractures act as no-flow boundaries. Hence, placing fractures on boundaries guarantees that lateral flow boundaries do not influence the flow field. For symmetrical reasons, fracture aperture of boundary fractures is adjusted so that their permeability is only half the permeability of fractures inside the domain. Starting with fracture spacing H (fracture level 1), fracture spacing is systematically halved to obtain the next fracture level. The densest fracture network (fracture level 6) consists of 65 vertical and 33 horizontal fractures including the four boundary half-fractures.

Each fractured HRL problem is compared to the base case. As the Rayleigh number is only applicable to homogeneous porous media, the equivalent permeability is used for comparison. The equivalent permeability k_{eq} (m^2) remains constant for each set of fracture networks. This is achieved by keeping matrix permeability constant and decreasing the fracture aperture whenever fracture spacing is decreased. The equivalent permeability in the z-direction (vertical) is calculated using the harmonic mean to include horizontal fractures and the arithmetic mean to include vertical fractures:

$$k_{eq} = (2B)\left(\frac{(2B)}{k_z} + \frac{(2b)}{k_f}\right)^{-1} \tag{2}$$

$$\text{with } k_z = k_M + \frac{k_f\,(2b)}{(2B)} \tag{3}$$

where $(2B)$ is the fracture spacing (m), k_f is the fracture permeability (m^2), and $(2b)$ is the fracture aperture (m). The permeability in the vertical direction with only vertical fractures considered is called k_z (m^2) and the matrix permeability is k_M (m^2). For the scenarios considered in this study, the horizontal fractures hardly influence k_{eq}. As fracture spacing is identical in both, the horizontal and vertical direction, the fractured medium is isotropic.

RESULTS

Modification of flow patterns

The influence of fractures on free convective flow is studied. Stepwise refined fracture networks are added to the base case, while retaining the equivalent permeability that corresponds to the Rayleigh number of 60. Two fractured cases are presented here, whose hydraulic parameters are listed in Table 1.

Table 1 Fracture networks and permeabilities for two fractured HRL settings. Equivalent permeability is $k_{eq} = 9.6 \times 10^{-16}\ m^2$ in all simulations.

		Case 1 $k_M = 9.0 \times 10^{-16}\ m^2$		Case 2 $k_M = 1.0 \times 10^{-16}\ m^2$	
Fracture level	fracture spacing (m)	fracture aperture (μm)	k_f/k_M ($\cdot 10^3$)	fracture aperture (μm)	k_f/k_M ($\cdot 10^3$)
1	10	19.4	35	46.9	1835
2	5	15.4	22	37.2	1156
3	2.5	12.2	14	29.6	728
4	1.25	9.7	9	23.5	459
5	0.625	7.7	6	18.6	289
6	0.3125	6.1	3	14.8	182

Matrix permeability for case 1 (9.0×10^{-16} m^2) is very similar to that of the unfractured HRL problem (9.6×10^{-16} m^2). Accordingly, fracture apertures are small such that fracture permeability contributes little to the equivalent permeability (k_{eq}). Matrix permeability for case 2 is 1/9 of the matrix permeability of case 1. Consequently, fracture apertures in case 2 are more than twice as large as in case 1 in order to retain k_{eq}. Thus, the k_f/k_M ratios for case 1 are much smaller than for case 2, as illustrated in Table 1.

Both cases are compared to the base case with the same equivalent permeability. The simulation results for the base case (isochlors and flow vectors) can be seen in Fig. 2. The local salt mass fraction at the horizontal cross section at half of the domain height was compared visually (Fig. 3(a),(b)) and by using the root mean square error (Fig. 4) in order to quantify differences.

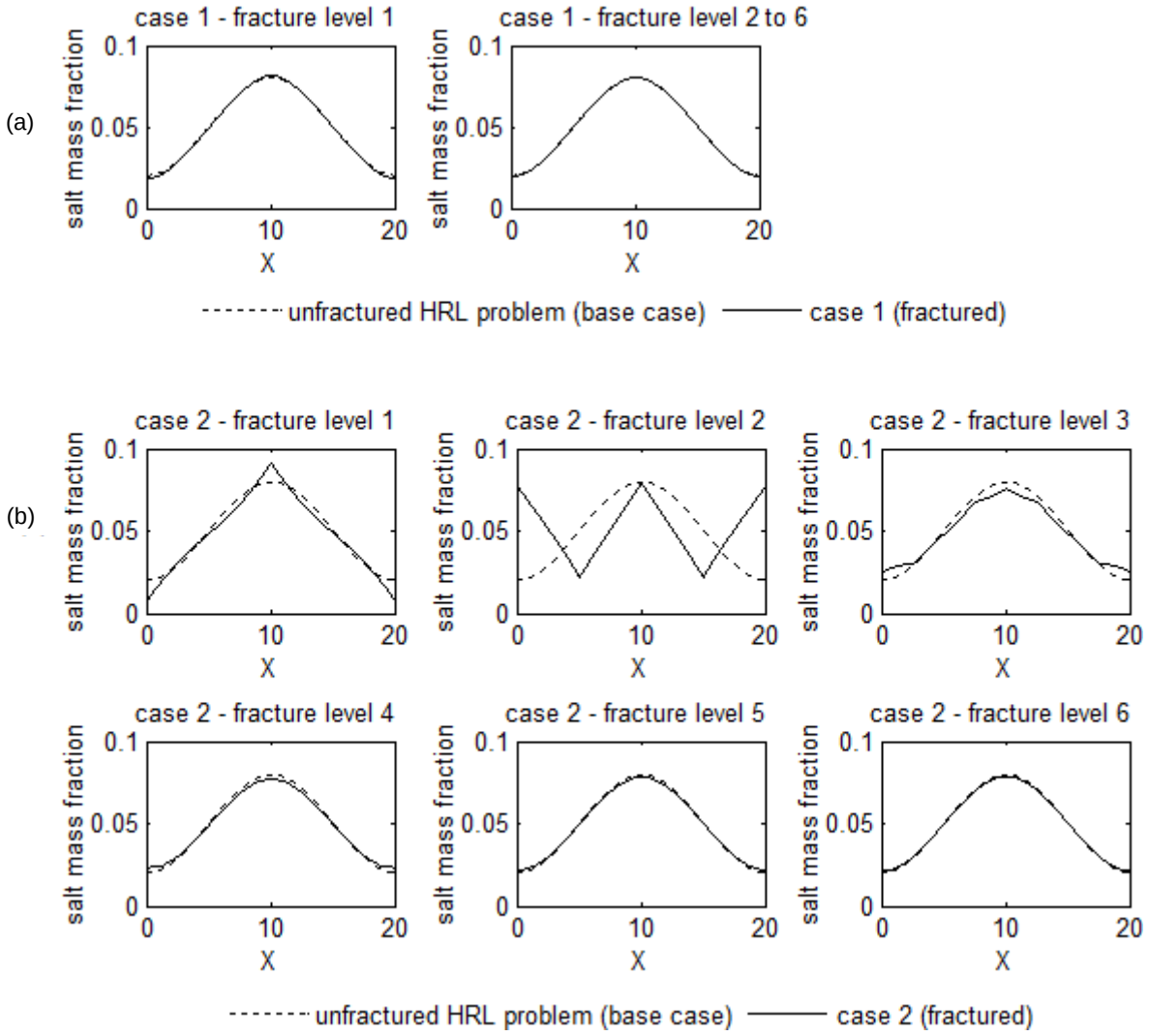

Fig. 3 (a) Salt mass fraction profile at cross section for case 1 (graphs for fracture level 2–6 are identical) and (b) salt mass fraction profile at cross section for case 2.

The two cases describe the transition zone between fractures being relevant to the flow patterns and fractures having only minor influence on the flow field. Most scenarios, including the unfractured base case, show upwelling at the lateral boundaries and central downwelling, which leads to the formation of two convections cells. Only fracture level 2 of case 2 has four convection

cells with downwelling in the centre and at the lateral boundaries and upwelling in and around the fractures at X = 5 m and X = 15 m. For each fracture level, the difference of the salt mass fraction profiles from the one of the unfractured HRL problem is much greater for case 2 than for case 1. The difference is greatest where the number of convection cells differs. The difference is small when fracture spacing is small and/or the contribution of fracture permeability to the equivalent permeability of the medium is minor, i.e. fracture aperture is small.

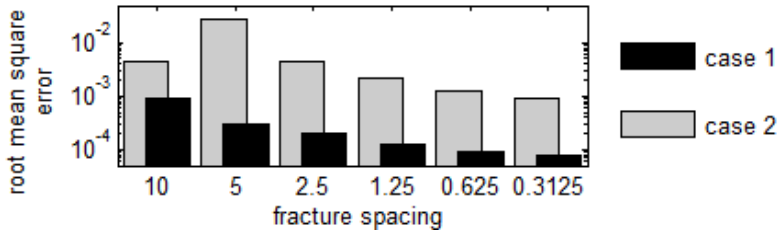

Fig. 4 Root mean square error (logarithmic y-axis) of salt mass fraction profiles, each case compared to unfractured HRL problem (base case).

Onset of convection

For the parameters used in this study, Ra_c is reached at an equivalent permeability of 6.32×10^{-16} m^2. For smaller permeabilities, the unfractured system is stable and purely diffusive. The fractured system, represented by the above mentioned case 2, was studied for equivalent permeabilities around that critical Rayleigh number. Matrix permeability is kept at 1×10^{-16} m^2 and fracture aperture is lowered to achieve smaller equivalent permeabilities. The results are compared using the mass flux through the top layer, expressed by the dimensionless Sherwood number (Sh). The Sherwood number compares total mass flux j (kg m^{-2} s^{-1}) for each simulation with the diffusive mass flux for the stable case. Sh is 1 for stable and purely diffusive systems and increases as free convection begins.

$$\mathrm{Sh} = \frac{\overline{j}}{D_0\,\theta\,\tau\,\rho_0\,(\Delta\omega / H)} \tag{4}$$

The Sherwood number is plotted *versus* equivalent permeability in Fig. 5 (Rayleigh number for the unfractured base case). For the fractured system with large fracture spacing (fracture level 1) the system becomes unstable at an equivalent permeability of 3.8×10^{-16} m^2 which is smaller than the one related to the critical Rayleigh number of $4\pi^2$. For intermediate fracture spacings (fracture

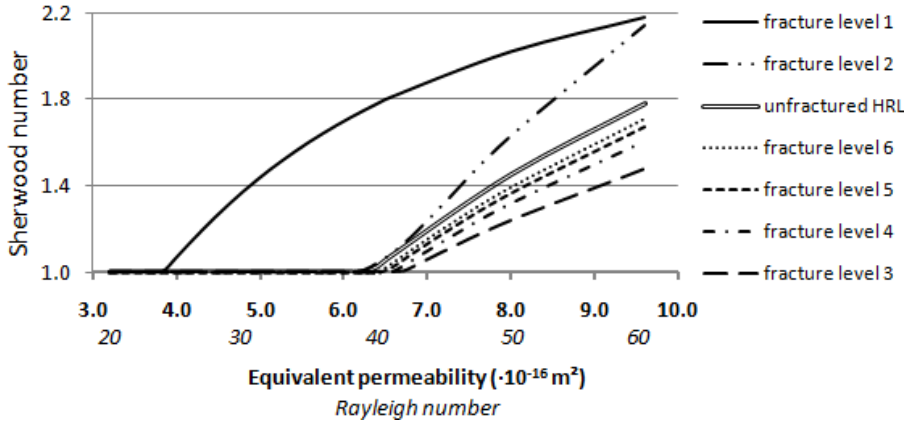

Fig. 5 Onset of convection: Sherwood number *versus* equivalent permeability and Rayleigh number. Fracture level 2 has four convection cells, unfractured HRL and all other fracture levels have two convection cells.

level 3), a higher equivalent permeability ($6.7 \cdot \times 10^{-16}$ m^2) than in the unfractured case is required to destabilize the system. For smaller fracture spacings and apertures, the required equivalent permeability for the onset of convection approximates that of the unfractured base case, as seen for fracture levels 4–6 in Fig. 5.

The total mass flux through the upper layer is not only dependent on the equivalent permeability, but differs for each fracture network. For fracture level 2, the system has a differing number of convection cells and therefore, the curve of the Sherwood number has a different shape.

CONCLUSIONS

Comparison of density dependent flow and transport in homogeneous and fractured porous media shows that orthogonal regular fracture networks do influence the modes of free convective flow, even if the equivalent permeability of the two media is identical. The influence of fractures increases with increasing fracture aperture and with decreasing fracture spacing. Different flow patterns and different rates of mass transport can result. Stability of the system is influenced by the presence of fractures. Sparsely spread orthogonal fractures promote free convection, while fracture networks with intermediate fracture spacing restrain it and denser orthogonal fracture networks hardly influence the onset of convection. Therefore, if dealing with fractured porous media, it is not sufficient just to know its equivalent permeability to predict free convective flow phenomena. The geometry of the fracture network has to be considered as well. The influence of artificial regular orthogonal fracture networks is presented here, but more realistic irregular networks require further research.

REFERENCES

Graf, T. & Therrien, R. (2007) Variable-density groundwater flow and solute transport in irregular 2D fracture networks. *Adv. Water Res*. 30, 455–468.

Horton, C. W. & Rogers, F. T. (1945) Convection currents in a porous medium. *J. Appl. Phys.* 16, 367–370.

Lapwood, E. R. (1948) Convection of a fluid in a porous medium. *Proc Cambridge Philos Soc*. 44, 508–521.

Therrien, R., McLaren, R. G., Sudicky, E. A. & Panday, S. M. (2010) HydroGeoSphere – a three-dimensional numerical model describing fully-integrated subsurface and surface flow and solute transport (manual). Groundwater Simulations Group, University of Waterloo, Canada.

van Reeuwijk, M., Mathias, S. A., Simmons, C. T. & Ward, J. D. (2009) Insight form a pseudospectral approach to the Elder problem. *Water Resour. Res.* 45, W04416.

Weatherill, D., Simmons, C. T., Voss, C. I. & Robinson, N. I. (2004) Testing density-dependent groundwater models: two-dimensional steady state unstable convection in infinite, finite and inclined porous layers. *Adv. Water Resour*. 27, 547–562.